THE JOURNAL OF BIOLOGICAL CHEMISTRY VOL. 285, NO. 4, pp. 2707–2720, January 22, 2010
Printed in the U.S.A.

Direct Observation of the Uncapping of Capping Protein-capped Actin Filaments by CARMIL Homology Domain 3*[S]

Received for publication, June 9, 2009, and in revised form, November 17, 2009 Published, JBC Papers in Press, November 19, 2009, DOI 10.1074/jbc.M109.031203

Ikuko Fujiwara, Kirsten Remmert, and John A. Hammer III[1]

From the Laboratory of Cell Biology, NHLBI, National Institutes of Health, Bethesda, Maryland 20892

Bulk solution assays have shown that the isolated CARMIL homology 3 (CAH3) domain from mouse and *Acanthamoeba* CARMIL rapidly and potently restores actin polymerization when added to actin filaments previously capped with capping protein (CP). To demonstrate this putative uncapping activity directly, we used total internal reflection microscopy to observe single, CP-capped actin filaments before and after the addition of the CAH3 domain from mouse CARMIL-1 (mCAH3). The addition of mCAH3 rapidly restored the polymerization of individual capped filaments, consistent with uncapping. To verify uncapping, filaments were capped with recombinant mouse CP tagged with monomeric green fluorescent protein (mGFP-CP). Restoration of polymerization upon the addition of mCAH3 was immediately preceded by the complete dissociation of mGFP-CP from the filament end, confirming the CAH3-driven uncapping mechanism. Quantitative analyses showed that the percentage of capped filaments that uncapped increased as the concentration of mCAH3 was increased, reaching a maximum of ~90% at ~250 nM mCAH3. Moreover, the time interval between mCAH3 addition and uncapping decreased as the concentration of mCAH3 increased, with the half-time of CP at the barbed end decreasing from ~30 min without mCAH3 to ~10 s with a saturating amount of mCAH3. Finally, using mCAH3 tagged with mGFP, we obtained direct evidence that the complex of CP and mCAH3 has a small but measurable affinity for the barbed end, as inferred from previous studies and kinetic modeling. We conclude that the isolated CAH3 domain of CARMIL (and presumably the intact molecule as well) possesses the ability to uncap CP-capped actin filaments.

Capping protein (CP)[2] is a highly conserved, ubiquitously expressed, heterodimeric actin-binding protein that plays a major role in limiting the duration of actin filament elongation within cells (1, 2). CP accomplishes this task by binding with high affinity (K_d ~ 0.1 nM) to the barbed end of the actin filament, thereby blocking the further association (and dissociation) of actin monomers at the fast growing end. CP is one of five proteins that are required for the reconstitution of actin polymerization-driven motility *in vitro* (3) Moreover, biochemical, cell biological, and modeling studies all suggest that rapid filament capping by CP *in vivo* is required in order to generate an Arp2/3-dependent dendritic actin network at the leading edge that is sufficiently branched to push the cell forward (4–7). Consistent with these studies, cells that lack CP or in which CP levels have been reduced exhibit profound alterations in the assembly of their actin cytoskeleton (8–12). Together, these observations highlight the necessity of identifying physiological regulators of CP function. A second compelling reason to search for such regulators stems from the very long half-time of CP at the barbed end *in vitro* (~30 min for vertebrate CP) (13, 14), because this half-time seems incompatible with the dynamics of actin *in vivo*, where large regions of F-actin can form and disassemble in seconds. Indeed, one recent study (15) estimated the average lifetime of CP on the barbed end *in vivo* to be ~1 s, or ~1,800-fold shorter than its *in vitro* half-time. These observations and considerations point to the possible existence within cells of a CP regulator(s) that dramatically accelerates the dissociation of CP from the barbed end.

One possible cellular regulator of CP function is CARMIL. CARMIL proteins comprise a recently identified family of molecules whose two most conspicuous features are a central, leucine-rich repeat domain and a C-terminal proline-rich domain (16, 17). Genes encoding CARMIL proteins have been identified in *Acanthamoeba*, *Dictyostelium*, *Caenorhabditis elegans*, *Drosophila*, mice, and humans (16–21). The first CARMIL protein to be identified was Acan125 (16). This 125-kDa *Acanthamoeba* protein was discovered based on its ability to bind to the isolated Src homology 3 domain of *Acanthamoeba* myosin-IC, a monomeric unconventional myosin. Using a similar approach, Jung *et al.* (17) subsequently identified p116, the *Dictyostelium* homologue of Acan125. Importantly, the eluates of their myosin I Src homology 3 domain affinity columns contained not only p116 but also CP and the Arp2/3 complex. Immunoprecipitation reactions and other experiments provided evidence that p116 forms a complex with

* This work was authored, in whole or in part, by National Institutes of Health staff.

[S] The on-line version of this article (available at http://www.jbc.org) contains supplemental Figs. S1 and S2 and Videos 1–3.

[1] To whom correspondence should be addressed: Laboratory of Cell Biology, Bldg. 50, Rm. 2523, NHLBI, National Institutes of Health, 9000 Rockville Pike, Bethesda, MD 20892-8017. Tel.: 301-496-1001; Fax: 301-402-1519; E-mail: hammerj@nhlbi.nih.gov.

[2] The abbreviations used are: CP, capping protein; CAH1 to -3, CARMIL homology domain 1–3, respectively; GST, glutathione *S*-transferase; mCARMIL-1, mouse CARMIL-1; mCAH3, mouse CAH3; PIP_2, phosphatidylinositol 4,5-bisphosphate; TIRF, total internal reflection; DTT, dithiothreitol; TMR, tetramethylrhodamine 5-maleimide; MOPS, 4-morpholinepropanesulfonic acid; UHF, ultra-high fidelity; TEV, tobacco etch virus; NTA, nitrilotriacetic acid; GFP, green fluorescent protein; EGFP, enhanced green fluorescent protein; mGFP, monomeric green fluorescent protein; ITC, isothermal titration calorimetry.

CP, Arp2/3, and myosin I *in vivo* and that p116 serves as the scaffold for assembly of this complex by binding CP, Arp2/3, and myosin I at independent sites. Given its central role in forming the complex, Jung *et al.* (17) gave p116 the name CARMIL (for capping protein, Arp2/3, myosin I linker).

Subsequent efforts to purify *Acanthamoeba* CARMIL provided evidence that CARMIL interacts very tightly with CP (22). Specifically, CARMIL and CP were found to co-purify through a lengthy purification procedure that included ammonium sulfate fractionation, hydrophobic interaction chromatography, affinity chromatography, and anion exchange chromatography. Moreover, the mixture of CARMIL and CP that was obtained from these steps was minimally resolved by size exclusion chromatography despite the fact that these two proteins differ enormously in Stokes radius. Consistent with these observations, a GST fusion protein containing the C-terminal ~200 residues of *Acanthamoeba* CARMIL was found to bind CP with an affinity of ~10 nM (23).

Sequence alignments identify three regions of strong similarity within CARMIL family proteins that we refer to as CARMIL homology domains 1–3 (CAH1–CAH3) (23). Recent studies of both *Acanthamoeba* CARMIL (23) and mouse CARMIL-1 (the product of one of three mouse CARMIL genes) (21) have established that the CAH3 domain forms the core of the CARMIL CP binding site. In the case of *Acanthamoeba* CARMIL, the ~30-residue CAH3 domain falls very near the protein's C terminus, and the isolated C-terminal 51 residues of *Acanthamoeba* CARMIL, which contains the protein's entire CAH3 domain sequence, binds CP very tightly (K_d ~10 nM by pull-down assay) (23). In the case of mouse CARMIL-1, mapping studies localized its CP binding site to an internal 123-residue fragment that encompasses the protein's CAH3 domain (21). This fragment, which is referred to as C1, was estimated by kinetic modeling to bind CP with an affinity of ~1.5 nM (21). Consistent with this estimate, our version of the minimal mCARMIL-1 CP binding site, which comprises essentially the N-terminal 74 residues of C1 (including all of the CAH3 domain) and which we refer to here as mCAH3, binds CP with an affinity of ~1 nM as determined by ITC.[3] For all of these active CARMIL fragments, conversion of a highly conserved arginine residue present in the center of the CAH3 sequence to a glutamate residue essentially abrogates their interaction with CP (21, 23) (in the case of mCAH3, the affinity of the Arg → Glu mutant for CP drops to ~1.5 μM, as determined by ITC).[3]

Bulk solution assays performed using CAH3 domain-containing fragments from both *Acanthamoeba* CARMIL (23) and mouse CARMIL-1 (21) argue strongly that this domain potently antagonizes CP function in two ways. First, assays in which CAH3 and CP are mixed together and then added to actin assembly assays indicate that the binding of CAH3 to CP dramatically reduces the affinity of CP for the barbed end. For the protozoan CAH3 domain, the complex of CAH3 and CP was estimated to bind the barbed end with an affinity of ~150 nM, down ~1,000-fold relative to CP alone (23). For the mouse CAH3 domain, the complex of C1 and CP was estimated to bind the barbed end with an affinity of ~15 nM, down ~100-fold relative to CP alone (21) (note that although the inhibition of CP capping activity by CAH3 is profound, the complex of CAH3 and CP still retains some capping activity; for this reason, we do not refer to this aspect of CAH3 behavior as sequestering, which should be restricted to situations in which regulator-CP interaction completely blocks CP capping activity (*e.g.* V-1·CP complex (24)). Second, assays in which the CAH3 domain is added to actin filaments previously capped with CP are consistent with the CAH3 domain-catalyzed removal of CP from the barbed end (*i.e.* with CAH3-driven uncapping). Importantly, the rapidity of this effect (in the case of the protozoan CAH3 domain, the addition of a 10-fold molar excess of CAH3 over CP resulted in a restoration in the rate of polymerization of previously capped actin filaments to near the seed-only rate in less than 10 s) argues strongly that the CAH3-dependent acceleration of the dissociation of CP from the barbed end is due to the binding of CAH3 to CP at the barbed end, which results in a rapid and large decrease in CP affinity for the filament end (as opposed to a mechanism in which free CAH3 in the assay serves merely as a sink for the slow, spontaneous dissociation of CP from the barbed end) (21, 23). This type of uncapping mechanism, where the binding of CAH3 to CP on the barbed end results in a large increase in the off-rate of CP from the end, would be completely consistent with the fact that the preformed complex of CP and CAH3 still binds the barbed end but very weakly.

Bulk solution assays performed previously are also consistent with the idea that micelles of phosphatidylinositol 4,5-bisphosphate (PIP_2), like the CARMIL CAH3 domain, inhibit the capping activity of free CP and catalyze the removal of CP from capped filament ends (14, 25). Using total internal reflection (TIRF) microscopy to visualize the capping and uncapping of single actin filaments *in vitro*, Kuhn and Pollard (13) recently confirmed that PIP_2 micelles antagonize the capping activity of free CP. Moreover, they obtained association and dissociation rate constants for mouse CP and the barbed end using these single molecule measurements that are in excellent agreement with rates measured previously using bulk solution assays. Importantly, however, they found no evidence in their TIRF-based assays that PIP_2 micelles accelerate the dissociation of CP from the barbed end of filaments previously capped with CP. The authors reconciled this result with the results of solution-based assays, which are consistent with PIP_2-driven uncapping, by showing that the generation of free barbed ends resulting from the shearing/severing of actin filament that occurs during the performance of solution-based assays, coupled with the sequestration of the free CP in the assay by PIP_2 micelles (so that the free ends generated by filament breakage are not capped), results in an increase in actin polymerization upon the addition of PIP_2 to capped filaments that gives the appearance of PIP_2-driven uncapping. Given their results, the authors suggested that the apparent uncapping activity of CARMIL, as observed in bulk solution assays (21, 23), should be verified at the single filament level. This important suggestion spawned the experiments described in this paper.

[3] T. Uruno, G. Piszczek, and J. A. Hammer III, manuscript in preparation.

EXPERIMENTAL PROCEDURES

Actin and Myosin—Actin was purified from rabbit skeletal muscle as described previously (26). Only the trailing fractions of G-actin from the S-300 gel filtration column, which lack oligomers that nucleate polymerization, were used. G-actin was stored in G-buffer (0.2 mM ATP, 1 mM NaN_2, 0.1 mM $CaCl_2$, 0.5 mM DTT, and 2 mM Tris-HCl (pH 8.0)). Mg-actin in KMEI buffer (50 mM KCl, 1 mM $MgCl_2$, 1 mM EGTA, 10 mM imidazole (pH 7.0)) was labeled with tetramethylrhodamine 5-maleimide (TMR) (Invitrogen) and purified by centrifugation, dialysis, and gel filtration as described elsewhere (27). The concentrations of actin and TMR were estimated using the extinction coefficients $A_{290} = 26{,}600\ \text{M}^{-1}\ \text{cm}^{-1}$ and $A_{550} = 96{,}900\ \text{M}^{-1}\ \text{cm}^{-1}$, respectively (28). The concentration of labeled actin was determined by subtracting 0.208 times the A_{550} value from the A_{290} value. TIRF experiments were performed using 20% labeled actin prepared by mixing equal concentrations of TMR-labeled actin and unlabeled actin at a volume ratio of 1:4. G-actin was labeled with pyrene, purified, and stored at −80 °C as described previously (29). The concentration of pyrene-labeled actin was determined by subtracting 0.127 times the A_{344} value from the A_{290} value. The concentration of pyrene was determined using $A_{344} = 22{,}000\ \text{M}^{-1}\ \text{cm}^{-1}$ (30). Solution assays were performed using 10% pyrene-labeled actin. Rabbit skeletal muscle myosin was prepared as described previously (31). The myosin was dialyzed into myosin buffer (0.5 M KCl and 10 mM MOPS (pH 7.0)), adjusted to a concentration of 4 μM, and inactivated by incubation at room temperature for 40 min with *N*-ethylmaleimide (Sigma) at a final concentration of 5 mM. DTT was added to a final concentration of 25 mM to stop the reaction. To collect the inactivated myosin, 10 volumes of distilled water were added to cause the myosin to assemble into filaments. The resulting myosin polymers were collected by centrifugation for 10 min at 5,000 × *g*. Following three washes of the pellet with distilled water, the myosin was solubilized in myosin buffer (0.5 M KCl, 1 mM DTT, and 10 mM MOPS (pH 7.0)), dialyzed into myosin storage buffer (myosin buffer supplemented with 50% glycerol), and stored at −20 °C. The concentration of the myosin was estimated using the extinction coefficient $A_{280} = 260{,}000\ \text{M}^{-1}\ \text{cm}^{-1}$ (13).

mCAH3—mCAH3, the minimal CAH3 domain fragment from mCARMIL-1 (GenBank™ AAR96060) used in this study, corresponds to residues 965–1038 of mCARMIL-1 or essentially the N-terminal 74 residues of C-1 (residues 962–1084), the 123-residue, CAH3 domain-containing mCARMIL-1 fragment used previously by Yang *et al.* (21). The experiments that led to the choice of residues 965–1038 for mCAH3, which span what we term the a and b subdomains of the mCARMIL1 CAH3 domain, will be described elsewhere.[3] In terms of the overall strategy to generate the mCAH3 protein, we placed the coding sequence for mCAH3 downstream of GST and upstream from a His_6 tag to allow dual purification of the peptide. We also added a trytophan residue immediately before the first residue of mCAH3 to allow the determination of protein concentration by absorbance. This cassette was then cloned into a GST plasmid containing a TEV protease cleavage site just 5′ of the tryptophan residue to allow removal of the GST moiety (see below). The sequence of the final mCAH3 protein used in this study is shown in Fig. 1*D*. To create the mCAH3 expression plasmid, we used ultra-high fidelity (UHF) *Pfu* polymerase (Stratagene), a full-length cDNA for mCARMIL-1, as the template and the following primers: 5′-CGGGGATCCGTCCGGCAAGAGAAGCGAAGCTCGGGG-3′ and 5′-AAGCGAATTCTACACCTTCTTGGTGAAAAACTCATCTAC-3′. The amplified fragment was then purified using a QIAquick PCR purification kit (Qiagen), digested with BamHI and EcoRI, repurified, and cloned into the GST vector pGEX-TEV-Parallel 1. The insert in the final plasmid was verified by DNA sequencing. Site-directed mutagenesis (QuikChange, Stratagene) was used to convert the arginine residue at position 993 that is critical for interaction with CP (21, 23) to a glutamate residue. The presence of the mutation was confirmed by DNA sequencing.

The large scale expression of GST- and histidine-tagged mCAH3 and its initial purification on glutathione-Sepharose 4B beads (Amersham Biosciences) were performed exactly as described recently for an earlier version of GST-tagged mCAH3 lacking the TEV cleavage site and the C-terminal histidine tag (32). Although some control experiments were performed using the resulting GST-tagged protein (see supplemental Fig. S1*E*), most experiments were performed using the protein following the removal of the GST moiety and a second purification step using the remaining histidine tag. To obtain such GST-free mCAH3, 1 ml of glutathione-Sepharose 4B beads charged with ~6 mg of GST-mCAH3 was washed five times with phosphate-buffered saline and two times with TEV digestion buffer (150 mM NaCl, 0.5 mM EDTA, 1 mM DTT, and 50 mM Tris-HCl (pH 8.0)) (10 ml/wash), resuspended in 1 ml of TEV digestion buffer, and digested for 2 h at room temperature with gentle rotation using 4 μl (40 units) of AcTEV protease (Invitrogen). Separate experiments determined that this amount of TEV protease was sufficient to digest >80% of the bound fusion protein in 2 h. The liberated fusion protein was collected as a flow-through by washing the resin in a small column using 2 ml of Ni^{2+}-NTA binding buffer (300 mM NaCl, 1 mM β-mercaptoethanol, 10 mM imidazole (pH 8.0), and 50 mM sodium phosphate (pH 8.0)). This material was then immediately added to 1 ml of Ni^{2+}-NTA beads (Qiagen) suspended in 5 ml of Ni^{2+}-NTA binding buffer and incubated for 1 h at 4 °C. After washing the beads three times (15 ml each) with Ni^{2+}-NTA washing buffer (same as binding buffer except containing 20 mM imidazole (pH 8.0)), GST-free mCAH3 was eluted using Ni^{2+}-NTA elution buffer (same as binding buffer except containing 160 mM imidazole (pH 8.0)). To separate mCAH3 from TEV protease, which is also present in the nickel column eluate because it also possesses a histidine tag, the eluate was rapidly dialyzed into Mono Q running buffer (50 mM KCl, 0.5 mM EDTA, 0.5 mM DTT, and 25 mM MOPS (pH 7.2)), loaded onto a 1-ml Mono Q column (Amersham Biosciences) equilibrated with Mono Q running buffer, and the column was washed with running buffer. This was sufficient to separate mCAH3 from the protease, because only the protease bound to the resin. The column flow-through was then concentrated using a Centricon concentrator and dialyzed against storage buffer (50 mM KCl, 1 mM $MgCl_2$, 1 mM EGTA, 0.5 mM DTT, and 10 mM imidazole (pH 7.0)). The GST-tagged version of mCAH3 used in a few

experiments was treated similarly. Protein concentrations were estimated using the following extinction coefficients: A_{280} = 49,850 M^{-1} cm^{-1} for GST-mCAH3 and A_{280} = 5,500 M^{-1} cm^{-1} for mCAH3. Densitometry of 4–20% SDS-polyacrylamide gels stained with Coomassie Blue indicated that GST-mCAH3 and mCAH3 were ~93 and ~96% pure, respectively. Both proteins were kept on ice and used for less than 2 weeks.

To generate a version of mCAH3 protein possessing a GFP tag for visualization in TIRF imaging, the coding sequence for the monomeric version of EGFP (mGFP), together with a His_6 tag at its N terminus for the purpose of purifying the chimeric protein, was fused to the N terminus of the coding sequence of mCAH3. To create this chimera, the coding sequence for mCAH3 flanked by XhoI and EcoRI sites was amplified using UHF *Pfu* polymerase and the following primers: 5′-ATAGTCCTCGAGGATCAGTCCGGCAAGAGAAGCGAAGC-3′ and 5′-TGAGAATTCTCACACCTTCTTGGTGAAAAACTCATCTACCCCTTCATCC-3′. The purified PCR product was then digested with XhoI and EcoRI and cloned into mEGFP-C1 (a monomeric version of EGFP-C1; gift of George Patterson (NICHD, National Institutes of Health)). A sequence-verified clone was then used as a template to amplify using UHF *Pfu* polymerase from the second residue of mGFP to the stop codon at the 3′-end of the mCAH3 coding sequence. The 5′-primer used began with a SacI site that is in frame with the N-terminal histidine tag present in the bacterial expression plasmid pET28a (Novagen), whereas the 3′-primer ended with a HindIII site. The specific primers used were 5′-TAGCAGAGCTCGTGAGCAAGGGCGAGGAGCTGTTCACC-3′ and 5′-GATACAAGCTTTCACACCTTCTTGGTGAAAAACTCATCTACCCCTTCATCC-3′. The purified PCR product was then digested with SacI and HindIII and cloned into pET28a. A sequence-verified clone was then transformed into competent BL21-RILP bacteria (Stratagene). The preparative expression of mGFP-mCAH3 and its purification on Ni^{2+}-NTA-agarose (Qiagen) were performed exactly as described previously for a histidine-tagged GFP-Rab27a fusion protein (33), except that GTP was not included in the buffers. The eluted protein was dialyzed into KMEI buffer supplemented with 0.5 mM DTT and 0.5 mM NaN_3 and used within 5 days. The concentration of mGFP-mCAH3 was determined by a Bradford assay.

Capping Protein—Recombinant, untagged mouse capping protein was expressed in *Escherichia coli* using a pET3a-based expression vector carrying in tandem the coding sequences for the mouse CP subunits α1 and β2 (34) (a kind gift from Dr. Pekka Lappalainen). The preparative expression of CP using this plasmid and its purification to homogeneity using a two-step procedure involving affinity purification on a resin charged with the CAH3 domain of mCARMIL-1, followed by anion exchange chromatography, were performed exactly as described recently (32). Pure CP was dialyzed into CP Buffer (50 mM KCl, I mM $MgCl_2$, 1 mM EGTA, 1 mM DTT, and 10 mM imidazole (pH 7.0)). For long term storage, CP was maintained at −20 °C in CP Buffer supplemented with 50% glycerol. The concentration of CP was estimated using the extinction coefficient A_{280} = 76,300 M^{-1} cm^{-1}.

To generate a version of mouse CP possessing a GFP tag for visualization in TIRF imaging, the coding sequence for mGFP was fused to the N terminus of the coding sequence for the β2 subunit of CP. To create this chimera, we switched to expression of CP using the plasmid pETDeut-1 (Novagen), which is designed specifically for the expression of two proteins in tandem. We first amplified the α1 subunit with NcoI/BamHI ends using UHF Pfu polymerase, the original CP expression plasmid (34), as the template and the following primers: 5′-TCATCCATGGCCGACTTTGAGGATCGGGTGTCGGAT-3′ and 5′-TGCGGATCCTTAAGCATTCTGCATTTCTTTGCCAATCTTGTAAC-3′. The resulting fragment was purified using a QIAquick PCR purification kit (Qiagen), digested with NcoI and BamHI, repurified, and cloned into the NcoI and BamHI sites within the MSC1 polylinker of pETDeut-1. The generation of the GFP-tagged version of the β2 subunit required several steps. First, the coding sequence for the β2 subunit was amplified as above but with SacI and EcoRI ends using the following primers: 5′-TAGACTGAGCTCAGAGTGGAGCTGGTAGCGATCAGCAGCTG-3′ and 5′-GATGAATTCTCAACACTGCTGCTTTCTCTTCAAGGCCTCCAC-3′. The resulting fragment was purified, digested with SacI and EcoRI, repurified, and cloned into the SacI and EcoRI sites of mEGFP-C1. The resulting plasmid was then used as a template to amplify from amino acid residue 2 of mEGFP to the stop codon of the β2 subunit using the following primers: 5′-TACGTACATATGGTGAGCAAGGGCGAGGAGCTGTTCACCG-3′ and 5′-ACTGTAGATATCTCAACACTGCTGCTTTCTCTTCAAGGCCTCCAC-3′. The resulting fragment was purified, digested with NdeI and EcoRV, repurified, and cloned into the NdeI and EcoRV sites within the MSC2 polylinker of the version of pETDeut-1 already harboring the α1 subunit in the MSC1 polylinker. Following sequence verification, this final expression plasmid was transformed into BL 21-RILP bacteria (Stratagene). The preparative expression, purification, and storage of mGFP-CP were performed exactly as described above for wild type CP (32). The concentration of mGFP-CP was estimated by densitometry of SDS-polyacrylamide gels loaded with mGFP-CP and wild type CP of known concentration to serve as a standard (and comparing the amounts of the α1 subunits for mGFP-CP and wild type CP).

Total Internal Reflection Microscopy—TIRF microscopy was performed using an objective lens-based TIRF system mounted on an Olympus IX-71 microscope (Olympus America) with a ×100 Plan Apo (numerical aperture 1.45) objective. An argon-krypton laser (568 nm) (Melles Griot) was used for tetramethylrhodamine excitation, and an argon laser (488 nm) (Melles Griot) was used for GFP excitation. Images were captured using a Spot-Boost EM-CCD camera (Diagnostic). The exposure time was always 0.5 s, and the time interval between frames varied from of 1 to 10 s (see details in the figure legends). A Z488/568 dichroic mirror (Chroma Technology) was used for two-color imaging. During two-color imaging, both lasers were used simultaneously, and the two signals were recorded using a Dual-View imager (Optical Insights). Two color images were overlaid using MetaMorph (Universal Imaging). The length of actin filaments was measured using ImageJ software (National Institutes of Health) (available on the World Wide Web) and a custom-designed plug-in written and generously provided by

Dr. Jeff Kuhn (Virginia Polytechnic Institute and State University).

TIRF-based Uncapping Assays—Cover glasses (number 1, 25 × 50 mm) were cleaned by sonication and acid and alkali wash as described previously (13, 26) to prevent the nonspecific binding of proteins. The flow cell was prepared by placing two pieces of double-sided cellophane tape in parallel onto a cover glass. A glass slide (25X75X1 mm, rinsed with water and air-dried) was then positioned perpendicularly across the cellophane tape to create a flow cell of ~7 μl. Solutions were loaded directly into the flow cell via capillary action. The performance of TIRF-based uncapping assays requires six steps (Steps 1–6; see Fig. 1 and "Results" for more details), all of which are carried out at 22 °C. In Step 1, 15 μl of a 50 nM solution of NEM-labeled rabbit skeletal muscle myosin in high salt buffer (500 mM KCl, 10 mM imidazole (pH 7.0)) is applied to the flow cell and incubated for 1 min. To block the glass surface and wash out excess NEM-myosin, 30 μl of a 1% (w/v) solution of BSA in KMEI buffer is applied to the flow cell in two 15-μl aliquots. In Step 2, 15 μl of 2 μM, 20% TMR-labeled actin solution in polymerization buffer (50 mM KCl, 1 mM $MgCl_2$, 1 mM EGTA, 10 mM imidazole (pH 7.0), 100 mM DTT, 0.2 mM ATP, 15 mM glucose, 0.5% (w/v) methylcellulose (1,500 CPI), 40 μg/ml catalase, and 200 μg/ml glucose oxidase) is applied to the flow cell. Filament formation is then observed for ~2 min to distinguish the barbed and pointed ends of each actin filaments. In Step 3, 15 μl of a 20 nM solution of CP in polymerization buffer is applied to the flow cell and incubated for 2 min (99.8% of filaments should be capped in this period of time using the association and dissociation rates of 2.6 $\mu M^{-1}\ s^{-1}$ and 0.0003 s^{-1} (13)). In Step 4, 15 μl of 2 μM, 20% TMR-labeled actin in polymerization buffer is applied to the flow cell, and the field is observed for ~1 min to identify those few filaments that have not been capped during Step 3. In Step 5, 15 μl of polymerization buffer is washed through the flow cell. In Step 6, 15 μl of a solution containing 2 μM, 20% TMR-labeled actin and various concentrations of mCAH3 in polymerization buffer is applied to the flow cell, and the flow cell is then viewed for 8.5 min. In some experiments, mGFP-CP was used instead of CP, and mGFP-mCAH3 was used instead of mCAH3. The mean and S.D. values for the data points in Figs. 2, 5*A*, and 5*B* were based on measuring at least 30 filaments from at least three independent experiments. Curve fitting was performed using KaleidaGraph software.

Solution-based Actin Polymerization—Solution-based actin polymerization assays using pyrene-labeled actin were performed at 22 °C essentially as described previously (13). Pyrene-labeled (100%) and unlabeled Ca-ATP actin monomers were mixed in G buffer to obtain a 10 μM stock solution that was 10% pyrene-labeled. To convert Ca-ATP actin monomers in this stock solution to Mg-ATP-actin monomers, a one-tenth volume of ME buffer (10 mM EGTA, 1 mM $MgCl_2$) was gently added, and the mixture was incubated for 2 min at room temperature. Actin polymerization (final actin concentration of 1 μM, diluted with G buffer) was initiated by adding actin seeds and 10× KMEI. Actin seeds were created by polymerizing 8 μM Mg-ATP G-actin at room temperature for 1 h and then vortexing aliquots for 20 s immediately before the addition to the assay. This sheared F-actin was added to the assay at a final concentration of 0.4 μM, which should correspond to ~0.4 nM barbed ends, based on calculations described previously (13). These values indicate that the average seed length was ~2.7 μm. Pyrene fluorescence was monitored with excitation at 365 nm and emission at 407 nm using a LS55 spectrophotometer (PerkinElmer Life Sciences). To measure the barbed end capping activities of untagged and mGFP-tagged CP, the proteins were mixed with actin seeds immediately before the seeds were added to the cuvette. To measure the ability of mCAH3 to inhibit the capping activities of CP and mGFP-CP, various concentrations of mCAH3 were mixed with CP (final concentration of 3 nM) at 10 times their final concentrations and incubated for 5 min at room temperature to form the complex of CP and mCAH3. These complexes were then diluted into 10% pyrene-labeled actin (final concentration of 1 μM). Actin seeds were then added immediately to start polymerization. To measure the ability of mCAH3 to uncap previously capped actin filaments, various concentrations of mCAH3 were added to assays containing 3 nM CP 1 min after polymerization had been initiated by the addition of actin seeds.

RESULTS

Establishment of the TIRF-based Uncapping Assay—Fig. 1*A* describes in schematic form the TIRF-based assay that we used to observe the uncapping of CP-capped actin filaments by mCAH3. Further details regarding this TIRF-based assay can be found under "Experimental Procedures" and in the legend to Fig. 1. Briefly, the glass surface of the flow chamber was first coated at low density with NEM-labeled rabbit skeletal muscle myosin in order to tether the actin filaments that formed in subsequent steps of the assay (Step 1). Following a washing step to remove unbound NEM-myosin and block nonspecific binding sites, 2 μM monomeric actin (20% TMR-labeled) in polymerization buffer was flowed into the chamber and allowed to assemble into filaments tethered by NEM-myosin (Step 2). The barbed and pointed ends of each tethered filament were easily distinguished based on their dramatic difference in assembly rate, with the elongation rate from the barbed end being much faster than from the pointed end in 2 μM actin (see legend to Fig. 1 for measured rate constants). Third, barbed ends were capped by flowing in 20 nM CP and incubating for 2 min (Step 3). Separate experiments demonstrated that >95% of the barbed ends in a typical field were capped within 30 s (supplemental Fig. S1*A*). Fourth, 2 μM monomeric actin (20% TMR-labeled) was flowed in, which also served to remove unbound CP (Step 4). This step allowed us to identify the small but measurable number of filaments in the field that had not been capped during Step 3, because only these never-capped filaments resume elongation at their barbed end upon performance of Step 4. Fig. 1*B* shows the barbed end (and pointed end) elongation kinetics for one such filament in *red*. In contrast to the behavior of a capped filament shown in *green*, the never-capped filament in *red* begins to elongate at its barbed end upon the addition of actin monomer in Step 4 (and prior to the addition of mCAH3 in Step 6, when the capped filament shown in *green* is uncapped and begins to elongate at its barbed end). These never-capped filaments, which represented 1–5% of the total filaments in a typical field, were eliminated from further analyses. Fifth, free actin

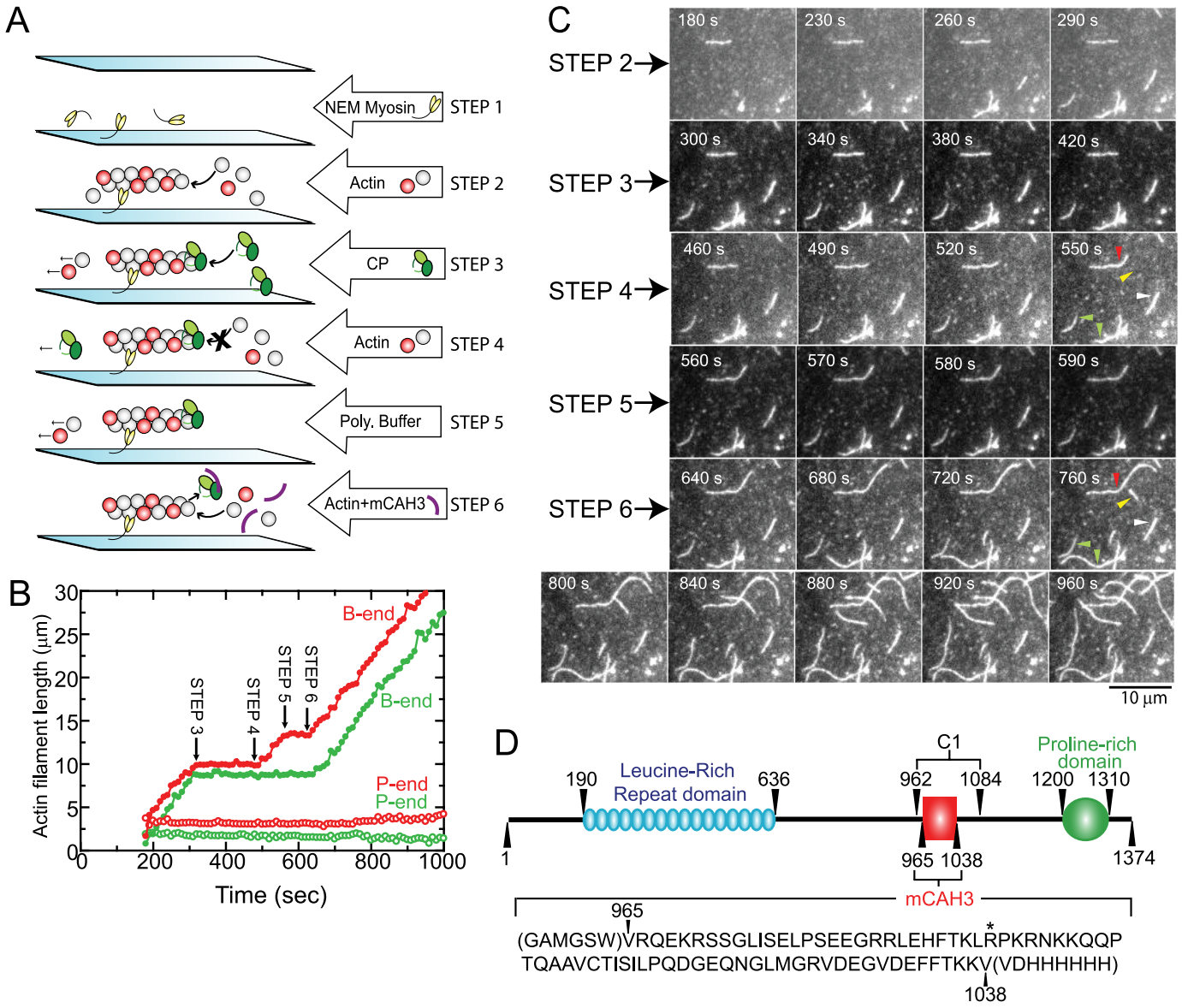

FIGURE 1. **Establishment of the TIRF-based uncapping assay.** *A*, schematic diagram of the steps that comprise our TIRF-based, single molecule uncapping assay (see "Experimental Procedures" and "Results" for details). Average elongation rates at the barbed and pointed ends of tethered filaments (2 μM actin) based on linear fitting were 22.39 ± 0.27 s^{-1} and 0.04 ± 0.11 s^{-1}, respectively ($n = 40$). *B*, time plots of the growth at the barbed (B-end; *filled symbols*) and pointed (P-end; *open symbols*) ends of two individual actin filaments, one of which (*red symbols*) was not capped at Step 3, as indicated by the fact that its barbed end began to grow again when actin monomer was added at Step 4, and one of which (*green symbols*) was capped at Step 3, as indicated by the fact that its barbed end did not elongate after Step 4. This latter filament resumed its elongation shortly after the addition of mCAH3 at Step 6. Solution exchanges are indicated by *arrows*. *C*, time series (time in *upper left corner*) of TIRF images in a typical uncapping assay performed using 30 nM mCAH3 in Step 6 (time 0 was the moment when actin was flowed into the chamber at Step 2). The *colored arrowheads* in the *rightmost panels* for Steps 4 and 6 point out examples of the four categories of filaments described. A movie (supplemental Video 1) containing the complete time series used to create *C* (in which images were taken every 5 s), is given in the supplemental material. *Scale bar*, 10 μm. *D*, schematic of the domain organization of full-length mCARMIL-1. The positions of the central leucine-rich repeat and C-terminal proline-rich domains are shown. Also shown are the positions of the CAH3 domain-containing fragment C1 used in (21) and our shorter version of C1, mCAH3. Shown *below* the schematic are the residues that comprise mCAH3 (along with a C-terminal histidine tag for purification and a short N-terminal extension that is retained after TEV cleavage and that contains a trytophan residue to allow the quantitation of mCAH3 protein amount by absorbance at 280 nm). The position of the critical arginine residue whose mutation to alanine or glutamate is function-blocking (21, 23) is marked by an *asterisk*.

monomer was removed by washing with polymerization buffer (Step 5). Finally, 2 μM monomeric actin (20% TMR-labeled) together with variable concentrations of mCAH3 were applied (Step 6), and the restoration of filament elongation at the barbed end was scored over an 8.5-min time interval (see Fig. 1*B*, *green symbols*, for an example of the barbed and pointed end elongation kinetics for a capped filament that uncapped shortly after the addition of mCAH3 at Step 6). This 8.5-min observational period was chosen because (i) solution-based measurements of the putative uncapping activity of mCAH3 (21, 23) (see below) indicate that this length of time is more than sufficient to estimate the uncapping activity of mCAH3 even at low concentrations of mCAH3, and (ii) beyond ~10 min, the density of actin filaments under our standard assay conditions becomes so high that quantitating the behavior of individual filaments becomes problematic due to filament overlap. In all

experiments, the total time interval between the end of Step 4 and the end of the 8.5-min observational period following Step 6 was kept precisely at 10 min in order to keep constant the contribution of the spontaneous dissociation of CP from the barbed end to total uncapping measured in the presence of mCAH3 (see below).

To quantify mCAH3-driven uncapping, all of the filaments in an individual field at the start and end of the 8.5-min observational period were placed into one of four categories: Category 1, filaments that began the observational period uncapped (*i.e.* that were never capped in Step 3) and that elongated during the observation period; Category 2, new filaments that appeared and elongated during the observation period; Category 3, filaments that began the observation period capped and never uncapped (*i.e.* never elongated) during the observation period; and Category 4, filaments that began the observation period capped but underwent uncapping and elongation sometime during the observation period. Fig. 1*C*, Steps 4 and 6 (see the images at 550 and 760 s), shows examples of all four filament categories in a typical field (*red arrowhead*, never capped (Category 1); *yellow arrowhead*, *de novo* growth (Category 2); *white arrowhead*, never uncapped (Category 3); *green arrowhead*, uncapped (Category 4) (see also supplemental Video 1). To quantify uncapping, Category 1 and 2 filaments were excluded, and the number of Category 4 filaments was divided by the sum of Category 3 and 4 filaments to obtain the fraction of capped filaments that underwent uncapping during the 8.5-min observational period. Importantly, this fraction represents a combination of both mCAH3-driven uncapping and the spontaneous dissociation of CP from the barbed end. Regarding the magnitude of the contribution of spontaneous CP dissociation to total uncapping measured in the presence of mCAH3, direct measurements of the rate of spontaneous dissociation of CP from the barbed end performed by Kuhn and Pollard (13) using a single molecule, TIRF-based assay like the one employed here indicate that ~14% of capped filaments should undergo spontaneous uncapping during our 8.5-min observational interval (based on their measured dissociation rate constant of 0.0003 s^{-1}) (13). Consistent with this estimate, we found in our TIRF-based uncapping assays that, in the absence of mCAH3, 10–15% of capped filaments underwent spontaneous uncapping during this 10-min interval (see Figs. 2 and 5 and supplemental Fig. S1*E*). As will become clear from measurements of the kinetics of mCAH3-driven uncapping in Fig. 3, this rate of spontaneous uncapping contributes very little to the rate of total uncapping measured at high concentrations of mCAH3.

Consistent with previous solution-based assays performed using the CAH3 domain from mice and *Acanthamoeba* CARMIL proteins (21, 23), mCAH3 had no effect on the rate of actin polymerization when assayed at the level of individual actin filaments observed by TIRF. Specifically, the barbed end elongation rate for individual actin filaments that had been uncapped by mCAH3 in the presence of 2 μM monomeric actin remained constant over a concentration range of 10–300 nM mCAH3 (supplemental Fig. S1*B*, *blue symbols*). Moreover, the average elongation rate for these uncapped filaments (22.6 ± 0.3 subunits/s) was indistinguishable from that exhibited by filaments before the addition of CP (22.4 ± 0.8 subunits/s; supplemental Fig. S1*B*, *red symbol*). Finally, we never observed in our TIRF images the severing of preexisting actin filaments upon addition of mCAH3 (even at high concentrations) (data not shown), and the addition of mCAH3 even at high concentrations did not result in an obvious increase in the number of spontaneously nucleating (Category 2) filaments (data not shown), arguing that mCAH3 does not nucleate actin polymerization, consistent with previous solution-based assays (21, 23).

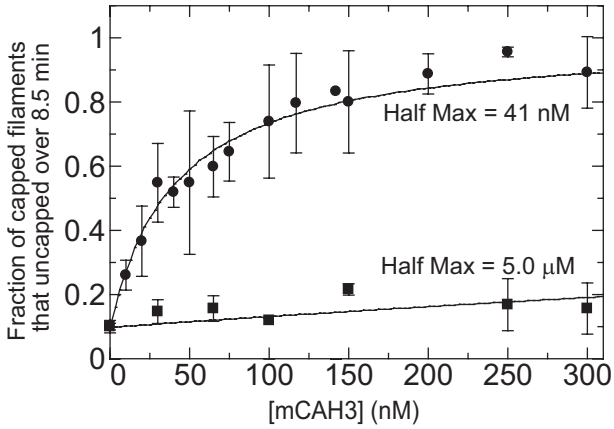

FIGURE 2. **Concentration dependence of the mCAH3-driven uncapping of CP-capped actin filaments.** Shown is the fraction of CP-capped filaments that uncapped during the 8.5-min observational period as a function of the concentration in the assay of either wild type mCAH3 (*filled circles*; half-maximal concentration (*Half Max*) 41 nM) or mCAH3 containing the function blocking mutation R993E (*filled squares*; half-maximal concentration 5.0 μM). For fitting, both curves were anchored using the value obtained in the absence of mCAH3 (~0.1 or ~10%, which is due to the spontaneous dissociation of CP over the 8.5-min observational window; see text).

Quantitative Analyses Reveal That mCAH3 Possesses Potent Uncapping Activity—As described in more detail under "Experimental Procedures," our mCAH3 fragment corresponds to an internal, 74-residue segment of C1, the 123-residue CAH3 domain-containing fragment from mCARMIL-1 that was used by Yang *et al.* (21) (Fig. 1*D*). Based on solution assays, the ability of mCAH3 to inhibit the capping activity of free CP and to uncap capped actin filaments is essentially identical to that reported for C1 (21), and the affinity of mCAH3 for CP, as measured by ITC, is similar to the value obtained for C1 using other methods (~1 nM).[3] As an example of the apparent uncapping activity exhibited by mCAH3 in a solution-based assay, supplemental Fig. S1*C* shows that the addition of mCAH3 to capped actin filaments in solution results in the rapid and dose-dependent restoration of the rate of polymerization toward the seed-only rate. Supplemental Fig. S1*D*, which plots the rate of polymerization as a fraction of the seed-only rate *versus* the concentration of mCAH3 added to the assay (which contained 3 nM CP), shows that the half maximal concentration of mCAH3 was ~30 nM and that in the presence of saturating amounts of mCAH3, the polymerization rate is ~90% that of the seed-only rate. These solution-based assay results are very similar to those described previously for C1 (21) (see below, regarding the fact that the rate of polymerization in the presence of saturating amounts of mCAH3 and C1 does not result in complete rescue of the polymerization rate).

Fig. 2 shows that mCAH3 uncaps capped actin filaments in a concentration-dependent manner when assayed using the sin-

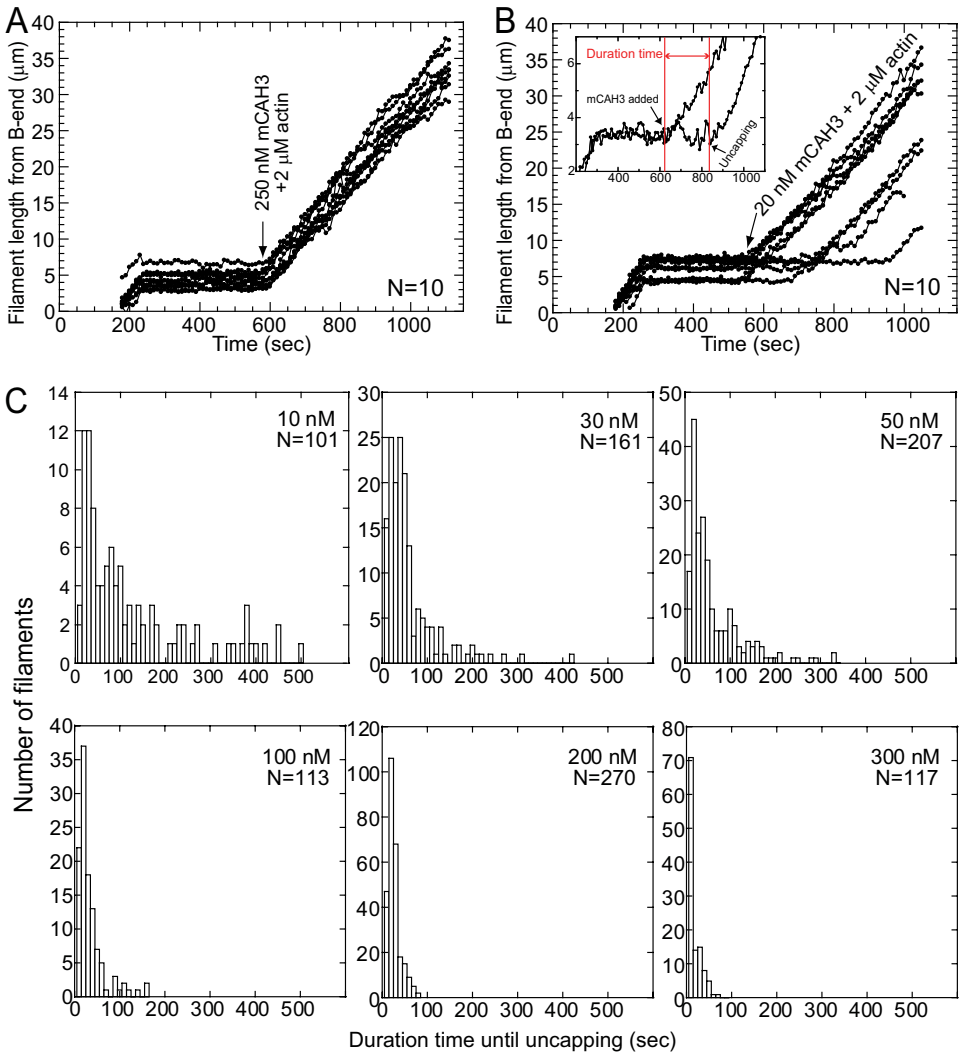

FIGURE 3. **Time interval between the mCAH3 addition and uncapping as a function of the concentration of mCAH3 added.** *A* and *B* show the time courses of elongation at the barbed end during our standard 8.5-min observational period for 10 randomly chosen capped actin filaments following the addition (see *arrows*) of either 250 nM mCAH3 (*A*) or 20 nM mCAH3 (*B*). The *inset* in *B* indicates how the "duration time until uncapping" used in *C* was measured (*i.e.* the time interval between the addition of mCAH3 and the resumption of elongation at the barbed end). *C* shows the cumulative data for the duration time until uncapping at six different concentrations of mCAH3. These concentrations as well as the total number of filaments examined at each concentration are indicated in the *upper right corner* of each histogram. Although we occasionally observed pauses in the barbed end elongation of uncapped actin filaments (see *A* and *B*), the frequency of such pauses was similar between actin filaments that never saw CP and actin filaments that saw 20 nM CP, a wash step, and then mCAH3 (either low or high concentrations) (data not shown), suggesting that these pauses are due largely to a surface effect (electrostatic and/or steric) rather than to recapping. Such surface effects have been reported by others (*e.g.* see Ref. 13). Although such paused filaments can resume growth, only the first incidence of growth resumption was used to score the duration time until uncapping as well as the data in Fig. 2.

gle molecule, TIRF-based assay described above. Specifically, the fraction of capped filaments that uncapped during the entire 8.5-min observational period following Step 6, as inferred from the restoration of growth at their barbed end, rose from ~0.1 (10%) in the absence of added mCAH3 (due to the spontaneous dissociation of CP from the barbed end) to ~0.90 (90%) in the presence of an amount of mCAH3 that is near or at saturation (>250 nM) (*closed circles*). The half-maximal concentration of mCAH3 for uncapping was ~41 nM. Mutation of the highly conserved arginine at position 993 in mCAH3 to glutamate (mCAH3 R993E), which completely blocks CAH3-driven uncapping in solution-based assays (21, 23) and which decreases the affinity of mCAH3 for CP by ~1,500-fold in ITC measurements,[3] almost completely abrogates the uncapping activity of mCAH3 in these single molecule assays (Fig. 2, *closed squares*; half-maximal concentration ~5.0 μM). We note that we obtained essentially identical results in uncapping assays using either unfused mCAH3 or GST-fused mCAH3 (both WT and the R993E mutant) (supplemental Fig. S1*E*). Unless indicated otherwise, unfused mCAH3 and mCAH3-R993E were used in the experiments reported here.

To better appreciate the potency of the uncapping activity of mCAH3, we quantified the time interval between the addition of mCAH3 (Step 6) and the moment of actin filament uncapping over a range of mCAH3 concentrations. Fig. 3, *A* and *B*, shows the polymerization traces for 10 randomly chosen, CP-capped actin filaments following the addition of either a high concentration of mCAH3 (250 nM) (*A*) or a low concentration of mCAH3 (20 nM) (*B*) (the *inset* in *B* indicates how the duration time between the mCAH3 addition and filament uncapping was determined from the polymerization trace). Although all 10 filaments uncapped (resumed growth) almost immediately following the addition of 250 nM mCAH3 (*A*), the uncapping of the 10 filaments following the addition of 20 nM mCAH3 (*B*) was spread out over ~6 min. Fig. 3*C* presents the cumulative data for the duration time between the mCAH3 addition and uncapping at six different concentrations of mCAH3 from 10 to 300 nM (the latter being a concentration that is near or at saturation, as determined in Fig. 2). The time lag between mCAH3 addition and uncapping is clearly concentration-dependent, decreasing dramatically and becoming much more tightly focused as the concentration of mCAH3 is raised. Moreover, at a concentration of mCAH3 that appears to be near or at saturation (300 nM), the duration time between the mCAH3 addition and uncapping becomes tightly focused around a value of ~10 s. This represents a mCAH3-driven acceleration in the rate of CP dissociation relative to the rate of spontaneous dissociation (half-time ~30 min) (13, 14) of at least 180-fold. These results are completely consistent with the very rapid res-

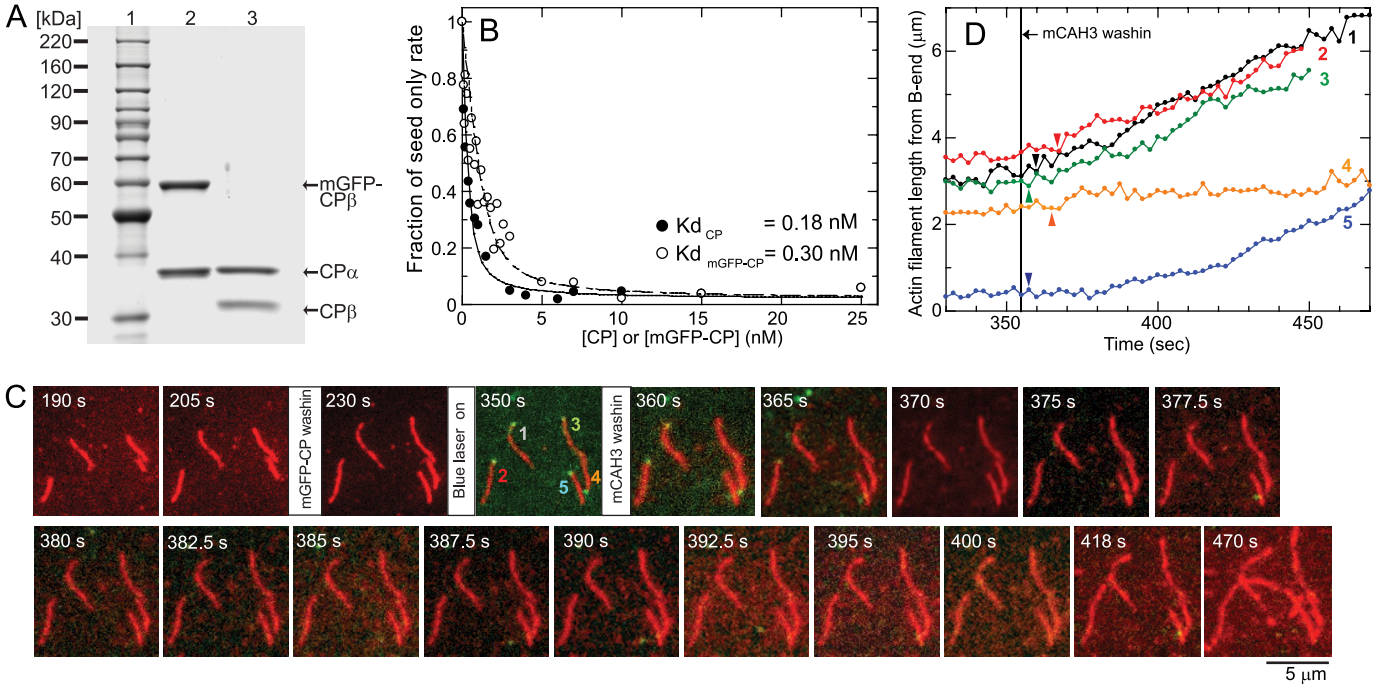

FIGURE 4. **Temporal correspondence between the disappearance of mGFP-CP from the barbed end and the reinitiation of filament elongation upon the addition of mCAH3.** *A*, Coomassie Blue-stained, 4–20% SDS-polyacrylamide gradient gel of molecular weight markers (*lane 1*), purified mGFP-CP (*lane 2*), and purified wild type CP (*lane 3*). *B*, shown are the barbed end capping activities of mGFP-CP (*open symbols*) and wild type CP (*filled symbols*), presented as fractions of the seed-only rate (1 μM actin, 10% pyrene-labeled). *C*, selected frames (time in *upper left corner*) from two-color TIRF imaging of single, rhodamine-labeled (20%) actin filaments that were capped with mGFP-CP and then incubated with 200 nM mCAH3. The timing of various additions and washes are indicated (see text for additional details). The blue laser for visualizing mGFP-CP was not turned on until 350 s to minimize the photobleaching of the molecule. A movie (supplemental Video 2) containing the complete time series used to create *C* (in which images were taken every 2.5 s) is given in the supplemental material. *Scale bar*, 5 μm. *D*, plots of the changes in length at the barbed end of the five filaments labeled in *C* following the addition of mCAH3 at 355 s (*vertical black line*). Also indicated using a *color-coordinated arrowhead* for each of these five filaments is the first frame where the green dot of mGFP-CP was no longer visible at the barbed end of the filament.

toration of actin polymerization observed in bulk solution-based uncapping assays using either protozoan (23) or mouse CAH3 domains (21) (supplemental Fig. S1*C*). That said, the quantitative analysis of mCAH3-driven uncapping shown in Fig. 3 is only possible using the direct observation of single actin filaments reported here.

Imaging Using Mouse CP Tagged with GFP Demonstrates that mCAH3 Drives the Complete Dissociation of CP from the Barbed End—Although the data in Figs. 2 and 3 provide strong support for the mCAH3-dependent uncapping of CP-capped actin filaments, the mCAH3-driven dissociation of CP from the barbed end is still simply inferred from the restoration of barbed end elongation measured in those experiments. To prove unequivocally that the restoration of elongation measured in Figs. 2 and 3 involves the actual mCAH3-driven removal of CP from the barbed end, we generated recombinant mouse CP $\alpha1\beta2$ in which mGFP was fused to the N terminus of the $\beta2$ subunit using a modification of the approach developed by Palmgren *et al.* (34) for the expression of mouse CP in *E. coli*. The recombinant CP, which we refer to below as mGFP-CP, was purified to homogeneity by affinity chromatography on a column of GST-mCAH3, followed by chromatography on Mono Q (Fig. 4*A*, *lane 2*; also see "Experimental Procedures"). Fig. 4*B* (*open circles*) shows that the affinity of mGFP-CP for the barbed end, as measured by the dose-dependent inhibition of actin polymerization from actin seeds, falls within the normal range measured for wild type mouse CP $\alpha1\beta2$ using the same assay (0.1–1.0 nM) (13, 14, 21). Specifically, the K_d values for three independent preparations of recombinant mGFP-CP were 0.35, 0.50, and 0.30 nM (the last is shown in Fig. 4*B* (*open circles*). These values, together with results obtained using wild type CP (*closed circles*; $K_d = 0.18$ nM), indicate that mGFP-CP is essentially as potent as wild type CP at capping the barbed end.

Fig. 4*C* shows video stills of a TIRF assay in which we examined in detail the temporal correspondence between the mCAH3-driven reinitiation of barbed end growth from red filaments capped with mGFP-CP and the disappearance of mGFP-CP from the barbed end (see also supplemental Video 2). At 230 s, 20 nM mGFP-CP was introduced into the flow cell. When the blue laser was turned on at 350 s, all five red actin filaments in the field (labeled *#1* through *#5*) had a green dot at one end, consistent with mGFP-CP capping their barbed end. At 355 s, 200 nM mCAH3 was introduced into the flow cell. By the time the next image was taken 5 s later (360 s), two of the five filaments (*#3* and *#5*) had lost the signal for mGFP-CP at their barbed end. By 365 s, only one filament (*#2*) retained the signal for mGFP-CP. Finally, by 370 s (*i.e.* only ~15 s after the initiation of the addition of mCAH3), the green dot of mGFP-CP had disappeared from the barbed end of all five filaments. Disappearance of the green dot could be due to the mCAH3-catalyzed dissociation of mGFP-CP from the barbed end or to the photobleaching of the molecule without its actual dissociation from the barbed end. To distinguish between these two possibilities, growth at the barbed end was measured for all five fila-

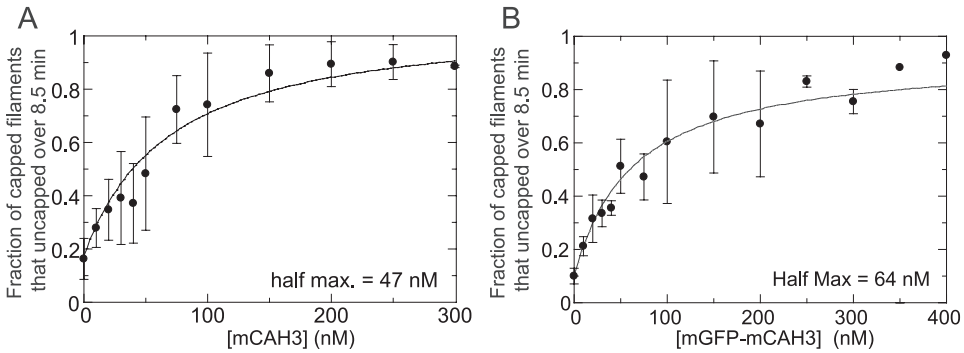

FIGURE 5. **Concentration dependence of the mCAH3-driven uncapping of mGFP-CP-capped actin filaments and the mGFP-mCAH3-driven uncapping of CP-capped actin filaments.** *A*, the fraction of filaments capped with mGFP-CP (as opposed to untagged CP as in Fig. 2) that uncapped during the 8.5-min observational period as a function of the concentration of mCAH3 in the assay (half-maximal concentration 47 nM). *B*, the fraction of CP-capped filaments that uncapped during the 8.5-min observational period as a function of the concentration in the assay of mGFP-mCAH3 (as opposed to untagged mCAH3 as in Fig. 2) (half-maximal concentration 64 nM). For fitting, both curves were anchored using the value obtained in the absence of mCAH3 (*A*) or mGFP-mCAH3 (*B*) (~0.16 or ~16% in *A* and ~0.07 or 7% in *B*, due to the spontaneous dissociation of mGFP-CP in *A* and CP in *B* over the 8.5-min observational window).

ments in the red channel from the moment of mCAH3 addition, because only the actual dissociation of mGFP-CP should be accompanied by the resumption of elongation. The results are plotted in Fig. 4*D* (the first frame where the green dot of mGFP-CP was no longer visible is marked for all five filaments by *color-coordinated arrowheads*). Based on regression analysis of the slopes of the barbed end elongation curves, filaments 1, 2, and 3 started growing essentially coincident with the addition of both mCAH3 and the disappearance of the green dot. Specifically, all three of these filaments resumed barbed end elongation within ~10 s after the initiation of mCAH3 washin and, more importantly, within 2.5 s (our imaging frequency) after the disappearance of the green dot of mGFP-CP from the barbed end. Close inspection of the barbed end elongation curve for filament 4 shows that it also resumed growth essentially coincident with the disappearance of mGFP-CP, although it stopped elongating shortly there after. Filament 5, on the other hand, represents what must be a clear example of the photobleaching of mGFP-CP without its dissociation from the barbed end, because this filament does not resume barbed end elongation until ~25 s after the disappearance from the barbed end of the fluorescent signal for mGFP-CP. To provide an estimate of the robustness of these results, we analyzed the barbed end elongation traces of 53 mGFP-CP-capped filaments following the mCAH3 addition (taken from five separate experiments). Of these 53 events, 30 showed unequivocal evidence of barbed end elongation within the three frames that immediately followed the first frame lacking the signal for mGFP-CP at the barbed end. For these events, therefore, the disappearance of the signal for mGFP-CP almost certainly represents the dissociation of the molecule from the barbed end rather than the photobleaching of the molecule without its dissociation. When we performed regression analysis on the growth curves for these 30 events, the average lag time between the disappearance of the signal for mGFP-CP and the resumption of growth at the barbed end was 2.1 ± 1.9 s. Given that mGFP-CP could have dissociated at any time during our 2.5-s imaging interval, we take this result as evidence that mCAH3-driven uncapping involves the simultaneous dissociation of CP from the barbed end and the resumption of barbed end elongation. We also note that we never observed a single example of the resumption of elongation at the barbed end while mGFP-CP was still present on the barbed end. Together, these results verify the mCAH3-driven uncapping mechanism by providing direct evidence that mCAH3 uncaps CP-capped actin filaments by driving the complete dissociation of CP from the barbed end.

Finally, although the data in Fig. 4 clearly show that mGFP-CP responds to mCAH3, we decided to quantify the sensitivity of mGFP-CP to mCAH3-driven uncapping in order to solidify the utility of mGFP-CP for future studies of CARMIL function (*e.g.* speckle microscopy *in vivo* to determine the half-life of CP at the barbed end). To accomplish this, we performed experiments like those shown in Fig. 2, except that the barbed end was capped with mGFP-CP rather than with wild type CP. For these experiments, uncapping was identified by the restoration of filament elongation in the red (rhodamine-actin) channel, as opposed to determining the time to dissociation of mGFP-CP in the green channel. This approach was used because the rates obtained using the latter approach were skewed significantly, especially at low concentrations of mCAH3, where the time lag between the mCAH3 addition and uncapping is very long, by the photobleaching of mGFP-CP (which results in mGFP-CP-capped filaments that lose the green dot at their barbed end but do not resume barbed end elongation).[4] Fig. 5*A* shows that, as with filaments capped with wild type CP (Fig. 2), mCAH3 uncaps filaments capped with mGFP-CP in a concentration-dependent manner. Specifically, the fraction of mGFP-CP-capped actin filaments that uncapped during the entire 8.5-min observation period following Step 6 rose from ~0.16 (~16%) in the absence of added mCAH3 (due to the spontaneous dissociation of mGFP-CP from the barbed end; note that this value is essentially identical to the value for wild type CP) to ~0.90 (90%) in the presence of an amount of mCAH3 that is near or at saturation (>250 nM) (*closed circles*). The half-maximal concentration of mCAH3 required for uncapping mGFP-CP-capped filaments was ~47 nM, which is very similar to the value obtained with CP-capped filaments (~41 nM; Fig. 2). We conclude, therefore, that two key biochemical properties of mGFP-CP (affinity for the barbed end and susceptibility to mCAH3-driven uncapping) are essentially identical to those of wild type CP.

[4] As evidence of the degree of bleaching, while the real half-time of mGFP-CP on the barbed end, as determined from the rate of resumption of growth of red filaments, is ~25 min (very similar to wild type CP), its half-time based on the lifetime of the green fluorescence dot on the barbed end drops to ~25 s because of the rapid bleaching of the mGFP-CP molecules that remain bound to the barbed end.

Imaging Using mCAH3 Tagged with GFP Supports the Existence of Transient Barbed End Capping by the Complex of CP and mCAH3—As mentioned in the Introduction, the complex of the CAH3 domain and CP appears to have measurable affinity for the barbed end (*i.e.* measurable capping activity). In other words, the CAH3 domain does not simply sequester CP in a complex that cannot interact with the barbed end (as happens, for example, when the CP regulator V-1/myotrophin binds to CP) (24). In the case of the CAH3 domain from mouse CARMIL-1, this affinity was estimated to be ~15 nM (21). Although this affinity is ~100-fold weaker than that of CP alone, it is far from insignificant and could be physiologically relevant (see "Discussion"). The weak capping activity of the complex of CP and CAH3 was first appreciated by Yang *et al.* (21) using bulk solution assays, where a saturating concentration of the C1 fragment from mCARMIL-1 restored the rate of actin polymerization to only ~85% that of the seed-only rate in assays in which C1 and CP were mixed together and then added to actin seeds. This behavior was also observed in uncapping assays where C1 was added to actin filaments that were already capped with CP (21). Indeed, as discussed below, this behavior is probably a signature of CP regulators that uncap CP rather than simply sequester CP.

Given the observations made by Yang *et al.* (21) and similar results that we obtained using our slightly smaller mCAH3 fragment in bulk solution assays (supplemental Fig. S1*D*; note that, like C1, the rate of polymerization in the presence of a saturating amount of mCAH3 is only ~85% of the seed-only rate), we sought to measure directly the lifetime of the complex of CP and mCAH3 at the barbed end by labeling mCAH3 with GFP. To accomplish this, the coding sequence for mGFP was fused to the N terminus of mCAH3. This fusion was then cloned into the expression plasmid pET28a, which provided a His_6 tag at the N terminus of the final fusion protein for purification purposes (see "Experimental Procedures"). Fig. 5*B* shows that the purified mGFP-mCAH3 fusion protein retains potent uncapping activity. Specifically, the half-maximal concentration of mGFP-mCAH3 required for uncapping CP-capped filaments (as assayed by the restoration of filament growth in the red rhodamine actin channel) was ~64 nM, which is fairly close to the value obtained for untagged mCAH3 and CP-capped filaments (~41 nM; Fig. 2). Given this result, we proceeded with experiments designed to measure the approximate lifetime of the complex of CP and mCAH3 at the barbed end by simultaneously imaging in the red (rhodamine actin) channel and green (mGFP-mCAH3) channel following the addition of mGFP-mCAH3 to red actin filaments capped with unlabeled CP. We looked specifically for events where a green dot could be seen to appear at the end of a capped red filament, followed sometime thereafter by the nearly simultaneous disappearance of this green dot and the reinitiation in the growth of the red actin filament. Such events presumably report the time interval between the association of GFP-tagged mCAH3 with a capped filament end and the dissociation of the complex of mGFP-mCAH3 and CP from this end (*i.e.* the lifetime of the complex of CP and mCAH3 at the barbed end). Events in which the green dot at the end of the filament disappeared without the subsequent reinitiation of filament growth, which could be due either

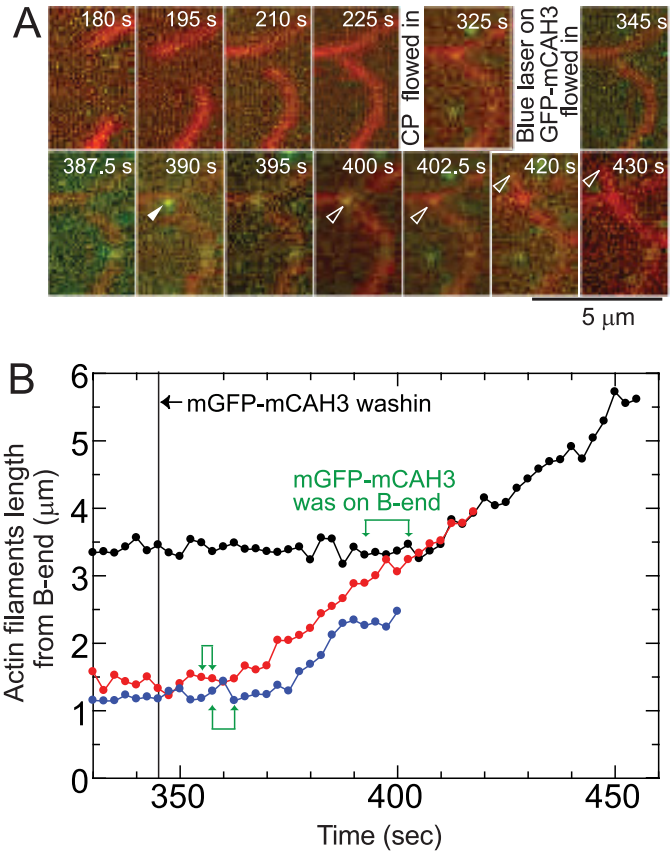

FIGURE 6. **mCAH3, viewed as a GFP chimera, resides briefly at the end of CP-capped filaments before dissociating along with CP.** *A*, selected frames (time in *upper right corner*) from two-color TIRF imaging of a single, rhodamine-labeled (20%) actin filament that was capped with unlabeled CP and then incubated with mGFP-mCAH3, resulting in the transient association of mGFP-mCAH3 with the barbed end, followed by uncapping and the reinitiation of barbed end elongation. The timing of various additions and washes is indicated (see text for additional details). The blue laser for visualizing mGFP-mCAH3 was not turned on until 345 s to minimize the photobleaching of the molecule. A movie (supplemental Video 3) containing the complete time series used to create *A* (in which images were taken every 2.5 s) is given in the supplemental material. *Scale bar*, 5 μm. *B*, plots of the changes in length at the barbed end of three CP-capped actin filaments following the addition of mGFP-mCAH3 at 345 s (*vertical black line*) (the *black symbols* correspond to the filament imaged in *A*). The *green bracket* associated with each filament trace indicates the time interval during which mGFP-mCAH3 was visible at the barbed end. In each case, the filament began elongating immediately after the disappearance of the GFP signal, arguing that in these instances the loss of the GFP signal was due to the dissociation of CP along with mGFP-mCAH3 (*i.e.* that these events report the residence time for the mGFP-mCAH3·CP complex at the barbed end).

to the bleaching of the mGFP-mCAH3 molecule without its dissociation from the barbed end or to its dissociation from the filament end as free mGFP-mCAH3 (*i.e.* not as an mGFP-mCAH3·CP complex), were discarded. Fig. 6*A* shows an example of an event where the duration of the complex of mGFP-mCAH3 and CP at the barbed end could be estimated. Specifically, the red filament in the center of the image, which grew at its barbed end between 180 and 225 s and which was then capped following the addition of CP at 225 s (based on the fact that its barbed end had not elongated when imaged ~100 s later at 325 s), acquired a green dot at its barbed end (see *filled white arrowhead* at 390 s) ~45 s after the addition of 10 nM mGFP-mCAH3 to the flow chamber at 345 s. Finally, this green dot disappeared 10–12.5 s later (present at 400 s, gone at 402.5

s; see *open white arrowheads* at 400 and 402.5 s), followed almost immediately by a measurable increase in the length of the actin filament at its barbed end in the red channel (see *open white arrowhead* at 420 and 430 s) (see also supplemental Video 3). All of the data points from imaging this filament at 2.5-s intervals following the addition of mGFP-mCAH3 are presented in graphical form in Fig. 6*B* (*black circles*). The *green bracket* spanning the time interval between 390 and 400 s marks the first and last frames where the green dot was visible at the barbed end of this filament. The results from two other independent events are also presented in similar fashion using *red* and *blue circles* (the time of addition of mGFP-mCAH3 to these samples was normalized to 345 s). Note that for all three events, a visual regression of the increase in actin filament length following the disappearance of the green dot of mGFP-mCAH3 shows that the transition from no growth (capped) to growth (uncapped) coincides almost exactly with the disappearance of mGFP-mCAH3 from the barbed end (presumably along with CP). The average lifetime of the complex of mGFP-mCAH3 and CP at the barbed end, based on a total of eight such events, was 9.2 ± 7.2 s. This large deviation is probably due to the relatively small N value ($n = 8$) as well as to the fact that our imaging frequency (2.5 s) is a significant fraction of the average dwell time for the complex at the barbed end. Nevertheless, the average value we obtained (~9 s) agrees well with the estimate of 10.5 s for the lifetime of the complex based on our kinetic modeling using rate constants and K_d values determined by us and by Yang *et al.* (21) (see supplemental Fig. S2, *A–C*, and the legend for supplemental Fig. S2). We conclude, therefore, that the single filament imaging presented in Fig. 6 using GFP-tagged mCAH3, like the bulk solution assays performed by us using mCAH3 and by Yang *et al.* (21) using C1, are consistent with the complex of mCAH3 and CP having measurable capping activity, a property that we think is consistent with the ability of the CAH3 domain to uncap CP-capped actin filaments.

DISCUSSION

The results of solution-based assays performed previously using CAH3 domain-containing fragments from both mouse CARMIL-1 (21) and protozoan CARMIL proteins (23) have been taken as evidence that this domain possesses the ability to uncap CP-capped actin filaments. Similar bulk solution assay results have been interpreted as evidence that micelles of PIP_2 also possess uncapping activity (13, 14, 25). Strikingly, a recent study using single molecule, TIRF-based assays showed that PIP_2 micelles are essentially devoid of uncapping activity (13) (however, see Fig. 6 in Ref. 25). Given this striking discrepancy for PIP_2, we sought here to confirm the uncapping activity of the CAH3 domain by single filament imaging. Our results show that the addition of mCAH3 rapidly restores the polymerization of individual, CP-capped actin filaments, which is consistent with uncapping. Moreover, we verified the CAH3-driven uncapping mechanism by directly imaging filaments capped with mouse CP tagged with mGFP, where the addition of mCAH3 led to the rapid and complete disappearance of mGFP-CP from the barbed end of the filament, followed immediately by the restoration of barbed end growth. Importantly, our single molecule assays show that mCAH3 accelerates the dissociation rate of CP from the barbed end at least 180-fold (from a half-time of ~30 min without mCAH3 to a half-time of ~10 s at a concentration of mCAH3 that is near or at saturation).

The ability of mCAH3 to dramatically increase the dissociation rate of CP from the barbed end requires that this domain form, over some finite period of time, a ternary complex with CP at the barbed end. Consistent with this, kinetic analyses (21) (supplemental Fig. S2), together with the direct determination of the mCAH3 dwell time at the end of capped actin filaments (Fig. 6), show that the complex of CP and mCAH3 possesses barbed end capping activity. Although this activity is much weaker than that of CP alone (~0.1 nM), it is measurable (estimated to be 15–30 nM for the complex of C1 and CP (21) and 38 nM for the complex of CP and mCAH3, based on kinetic analyses of data presented in part in this study (supplemental Fig. S2)), and it may be physiologically significant (see below). Together, these results argue that the binding of the CAH3 domain to CP on the barbed end results in a rapid and large decrease in the affinity of CP for the barbed end, leading to the rapid dissociation of the complex of CP and CAH3 from the filament end (*i.e.* to uncapping). The tight interaction of CP with the barbed end appears to be driven largely by the association of the C-terminal, flexible extensions of its α and β subunits (its α and β tentacles) with the filament end (for a review, see Refs. 1 and 2). Interestingly, measurements of the barbed end capping activities of versions of CP that lack either or both tentacles (35, 36) indicate that CP lacking its β tentacle possesses a dissociation rate from the barbed end that is roughly similar to the dissociation rate for the complex of CAH3 and CP. Given this and the fact that the tight interaction between the CAH3 domain and CP does not appear to involve contacts between CAH3 and either tentacle (the affinities of C1 for CP and for tentacle-free CP are essentially identical (21)), we speculate that the binding of CAH3 to the body of CP present at the barbed end promotes uncapping by inducing a conformational change in the structure of CP that results in the release of its β tentacle from the filament end. Determination of how the binding of CAH3 to CP induces such an allosteric effect resulting in rapid uncapping must await the determination of the structure of the complex of mCAH3 and CP. Such structural information should also shed further light on the mechanism by which CP caps the barbed end. Finally, given all of the results and considerations outlined above, it makes sense that V-1/myotrophin, which completely blocks the interaction of CP with the barbed end (24), is incapable of uncapping. Indeed, we speculate that proteins like V-1 that sequester CP will always be incapable of uncapping because uncapping requires that the protein form a transient ternary complex at the barbed end (*i.e.* that the complex of CP and the protein have some barbed end capping activity). Likewise, we imagine that proteins like CARMIL that possess uncapping activity will always be incapable of sequestering CP (although they will always reduce the affinity of CP for the barbed end).

Given the results described above for PIP_2 micelles, which show that these micelles sequester CP but do not uncap CP-capped actin filaments (13), CARMIL now appears to be the

only molecule proven to possess uncapping activity. However, the two other families of vertebrate proteins that possess CAH3 domains (the CD2AP/CIN85 adaptor proteins and the pleckstrin homology domain-containing CKIP proteins) may possess uncapping activity (37, 38). Indeed, solution-based assays performed with the CAH3 domain of CD2AP (37) are consistent with uncapping activity, but single molecule observations will be required to confirm this. Our belief is that CAH3 domains will always possess uncapping activity regardless of their protein context, although the potency of their uncapping activity may vary considerably, depending on the protein context.

Actin polymerization *in vivo* occurs primarily at the barbed end, so mechanisms that control the number of free barbed ends are crucial for the regulation of actin filament assembly within cells (39). Cells appear to use at least three mechanisms to generate free barbed ends for filament assembly (39). First, barbed ends are created *de novo* by the action of nucleating machines such as the Arp2/3 complex, the formins, and spire proteins. Second, free barbed ends are created by severing preexisting actin filaments through the action of proteins like cofilin and gelsolin. Finally, significant numbers of free barbed ends may be generated by the active removal of barbed-end cappers like CP from the end of preexisting, capped actin filaments. Our demonstration here that the CAH3 domain of mouse CARMIL-1 possesses uncapping activity suggests that CARMIL proteins (and possibly other CAH3 domain-containing proteins) may contribute, along with *de novo* nucleation and filament severing, to the generation of free barbed ends *in vivo*.

Using GFP-tagged CP and single molecule, *in vivo* speckle microscopy, Miyoshi *et al.* (15) reported recently that the average half-life of CP at the barbed end of actin filaments within the lamellipodia of *Xenopus* fibroblasts is ~1 s, which is ~1,800-fold shorter than the half-time of CP measured *in vitro* (~30 min). These authors suggested that the uncapping activity of cellular factors, such as PIP_2 and CARMIL, might be responsible for the very short half-life of CP at the barbed end *in vivo*. Given our results reported here and the results of Kuhn and Pollard (13) regarding PIP_2, the only known cellular source of such uncapping activity at present would be CARMIL. In thinking about the possible role of CARMIL proteins in regulating the residence time of CP at the barbed end of actin filaments *in vivo*, the issue of whether CARMIL proteins are regulated or constitutively active becomes very important, especially given the extremely high affinity of the CAH3 domain for CP (~1 nM) and the reported cellular concentrations of CARMIL (~2 μM) and CP (~1 μM) (21). Relevant to this issue, purified full-length protozoan CARMIL exhibits much weaker anti-CP activities than its isolated CAH3 domain (23), possibly because the full-length molecule is subject to autoinhibition resulting from some form of intramolecular folding. Presumably, full-length CARMIL is folded and inactive until it is unfolded and activated by some type of physiological activation event. Consistent with this, mCARMIL-1 possesses a CRIB-like sequence (23),[5] suggesting that it may fit the paradigm for other key regulators of actin assembly, such as WASPs and formins, where binding to a membrane-associated Rho GTPase serves to (i) unfold and activate the protein and (ii) to focus its activity at the plasma membrane/cytosol interface (39). It should be noted, however, that purified, full-length mCARMIL-1 has been reported to be just as active *in vitro* as its isolated CAH3 domain (21). If this is the case *in vivo*, then CARMIL may indeed be largely responsible for the very short average lifetime of CP on the barbed end *in vivo* measured by Miyoshi *et al.* (15). Importantly, CARMIL might drive this very short lifetime not only by uncapping CP-capped actin filaments but also by generating significant cytosolic levels of the complex of CP and CARMIL, which binds the barbed end weakly. The other distinct possibility is that full-length CARMIL is largely inactive *in vivo* (perhaps it is inhibited in *trans* by some factor) and that its activity is temporally and spatially restricted to regions of the cell that receive some sort of CARMIL-activating signal. In this case, the very short lifetime of CP in the lamellopodium would have to be due to some other property of the dendritic actin network. For example, based on the significant lengthening of the lifetime of CP speckles in cells overexpressing Lim kinase, Miyoshi *et al.* (15) argue that the short lifetime of CP throughout the lamellopodium is due, at least in part, to the rapid generation of short, freely diffusing, capped actin oligomers by cofilin-dependent severing.

Acknowledgments—We thank Xufeng Wu, Dimitris Vavylonis, Jeff Kuhn, Attila Nagy, Earl Homsher, P. Boon Chock, Edward D. Korn, and all members of the Hammer laboratory for comments and advice on this work. We also thank Pekka Lappalainen for the generous gift of the CP expression plasmid.

[5] S. McCroskery and J. A. Hammer III, unpublished observations.

REFERENCES

1. Wear, M. A., and Cooper, J. A. (2004) *Trends Biochem. Sci.* **29,** 418–428
2. Cooper, J. A., and Sept, D. (2008) *Int. Rev. Cell Mol. Biol.* **267,** 183–206
3. Loisel, T. P., Boujemaa, R., Pantaloni, D., and Carlier, M. F. (1999) *Nature* **401,** 613–616
4. Pollard, T. D., Blanchoin, L., and Mullins, R. D. (2000) *Annu. Rev. Biophys. Biomol. Struct.* **29,** 545–576
5. Akin, O., and Mullins, R. D. (2008) *Cell* **133,** 841–851
6. Iwasa, J. H., and Mullins, R. D. (2007) *Curr. Biol.* **17,** 395–406
7. Mogilner, A., and Edelstein-Keshet, L. (2002) *Biophys. J.* **83,** 1237–1258
8. Amatruda, J. F., Cannon, J. F., Tatchell, K., Hug, C., and Cooper, J. A. (1990) *Nature* **344,** 352–354
9. Amatruda, J. F., Gattermeir, D. J., Karpova, T. S., and Cooper, J. A. (1992) *J. Cell Biol.* **119,** 1151–1162
10. Sizonenko, G. I., Karpova, T. S., Gattermeir, D. J., and Cooper, J. A. (1996) *Mol. Biol. Cell* **7,** 1–15
11. Mejillano, M. R., Kojima, S., Applewhite, D. A., Gertler, F. B., Svitkina, T. M., and Borisy, G. G. (2004) *Cell* **118,** 363–373
12. Hug, C., Jay, P. Y., Reddy, I., McNally, J. G., Bridgman, P. C., Elson, E. L., and Cooper, J. A. (1995) *Cell* **81,** 591–600
13. Kuhn, J. R., and Pollard, T. D. (2007) *J. Biol. Chem.* **282,** 28014–28024
14. Schafer, D. A., Jennings, P. B., and Cooper, J. A. (1996) *J. Cell Biol.* **135,** 169–179
15. Miyoshi, T., Tsuji, T., Higashida, C., Hertzog, M., Fujita, A., Narumiya, S., Scita, G., and Watanabe, N. (2006) *J. Cell Biol.* **175,** 947–955
16. Xu, P., Mitchelhill, K. I., Kobe, B., Kemp, B. E., and Zot, H. G. (1997) *Proc. Natl. Acad. Sci. U.S.A.* **94,** 3685–3690
17. Jung, G., Remmert, K., Wu, X., Volosky, J. M., and Hammer, J. A., 3rd

(2001) *J. Cell Biol.* **153,** 1479–1497
18. Vanderzalm, P. J., Pandey, A., Hurwitz, M. E., Bloom, L., Horvitz, H. R., and Garriga, G. (2009) *Development* **136,** 1201–1210
19. Rogers, S. L., Wiedemann, U., Stuurman, N., and Vale, R. D. (2003) *J. Cell Biol.* **162,** 1079–1088
20. Matsuzaka, Y., Okamoto, K., Mabuchi, T., Iizuka, M., Ozawa, A., Oka, A., Tamiya, G., Kulski, J. K., and Inoko, H. (2004) *Gene* **343,** 291–304
21. Yang, C., Pring, M., Wear, M. A., Huang, M., Cooper, J. A., Svitkina, T. M., and Zigmond, S. H. (2005) *Dev. Cell.* **9,** 209–221
22. Remmert, K., Olszewski, T. E., Bowers, M. B., Dimitrova, M., Ginsburg, A., and Hammer, J. A., 3rd (2004) *J. Biol. Chem.* **279,** 3068–3077
23. Uruno, T., Remmert, K., and Hammer, J. A., 3rd (2006) *J. Biol. Chem.* **281,** 10635–10650
24. Bhattacharya, N., Ghosh, S., Sept, D., and Cooper, J. A. (2006) *J. Biol. Chem.* **281,** 31021–31030
25. Kim, K., McCully, M. E., Bhattacharya, N., Butler, B., Sept, D., and Cooper, J. A. (2007) *J. Biol. Chem.* **282,** 5871–5879
26. Kuhn, J. R., and Pollard, T. D. (2005) *Biophys. J.* **88,** 1387–1402
27. Fujiwara, I., Takahashi, S., Tadakuma, H., Funatsu, T., and Ishiwata, S. (2002) *Nat. Cell Biol.* **4,** 666–673
28. Houk, T.W., Jr., and Ue, K. (1974) *Anal. Biochem.* **62,** 66–74
29. Cooper, J. A., Walker, S. B., and Pollard, T. D. (1983) *J. Muscle Res. Cell Motil.* **4,** 253–262
30. Kouyama, T., and Mihashi, K. (1980) *Eur. J. Biochem.* **105,** 279–287
31. Kielly, W. W., and Harrington, W. F. (1960) *Biochim. Biophys. Acta* **41,** 401–421
32. Remmert, K., Uruno, T., and Hammer, J. A. (2009) *Protein Expr. Purif.* **67,** 113–119
33. Wu, X., Sakamoto, T., Zhang, F., Sellers, J. R., and Hammer, J. A., 3rd (2006) *FEBS Lett.* **580,** 5863–5868
34. Palmgren, S., Ojala, P. J., Wear, M. A., Cooper, J. A., and Lappalainen, P. (2001) *J. Cell Biol.* **155,** 251–260
35. Kim, K., Yamashita, A., Wear, M. A., Maéda, Y., and Cooper, J. A. (2004) *J. Cell Biol.* **164,** 567–580
36. Wear, M. A., Yamashita, A., Kim, K., Maéda, Y., and Cooper, J. A. (2003) *Curr. Biol.* **13,** 1531–1537
37. Bruck, S., Huber, T. B., Ingham, R. J., Kim, K., Niederstrasser, H., Allen, P. M., Pawson, T., Cooper, J. A., and Shaw, A. S. (2006) *J. Biol. Chem.* **281,** 19196–19203
38. Canton, D. A., Olsten, M. E., Niederstrasser, H., Cooper, J. A., and Litchfield, D. W. (2006) *J. Biol. Chem.* **281,** 36347–36359
39. Pollard, T. D., and Borisy, G. G. (2003) *Cell* **112,** 453–465